Submitted to ADVANCED MATERIALS

This document is the accepted manuscript version of the following article:
Sina Abdolhosseinzadeh, René Schneider, Anand Verma, Jakob Heier, Frank Nüesch and Chuanfang (John) Zhang*,* **Turning Trash into Treasure: Additive Free MXene Sediment Inks for Screen-Printed Micro-Supercapacitors,** Advanced Materials, **2020,** 2000716, **DOI: 10.1002/adma.202000716.**

Turning Trash into Treasure: Additive Free MXene Sediment Inks for Screen-Printed Micro-Supercapacitors

By *Sina Abdolhosseinzadeh, René Schneider, Anand Verma, Jakob Heier,* Frank Nüesch and Chuanfang (John) Zhang**

S. Abdolhosseinzadeh, Dr. R. Schneider, A. Verma, Dr. J. Heier, Prof. F. Nüesch, Dr. C. Zhang
Laboratory for Functional Polymers, Empa, Swiss Federal Laboratories for Materials Science and Technology, Überlandstrasse 129, CH-8600 Dübendorf, Switzerland
E-mail: jakob.heier@empa.ch; chuanfang.zhang@empa.ch

S. Abdolhosseinzadeh, Prof. F. Nüesch
Institute of Materials Science and Engineering, Ecole Polytechnique Fedérale de Lausanne (EPFL), Station 12, CH-1015 Lausanne, Switzerland

Abstract

Printed functional conductive inks have triggered scalable production of smart electronics such as energy storage devices, antennas, wearable electronics, etc. Of particular interest are highly conductive additive-free inks devoid of costly post deposition treatments to eliminate sacrificial components. Due to the high filler concentration required, formulation of such waste-free inks has proven quite challenging. Here, we demonstrate additive-free, two-dimensional titanium carbide MXene aqueous inks with appropriate rheological properties for scalable screen printing. Importantly, the inks consist essentially of the sediments of unetched precursor and multi-layered MXene, which are usually discarded after delamination. We present screen-printed structures on paper with high resolution and spatial uniformity, including micro-supercapacitors, conductive tracks, integrated circuit paths and others. We reveal that the delaminated nanosheets among the layered particles function as efficient conductive binders, maintaining the mechanical integrity and thus the metallic conductive network. The areal capacitance (158 mF/cm^2) and energy density (1.64 μWh/cm^2) of the printed micro-supercapacitors are much superior to other devices based on MXene or graphene. The ink formulation strategy of "turning trash into treasure" for screen-printing highlights the potential of waste-free MXene sediment printing for scalable and sustainable production of next-generation wearable smart electronics.

The advancement of smart electronics and internet of things (IoTs) have significantly stimulated the development of functional materials and devices,[1–3] in particular miniaturized supercapacitors (or micro-supercapacitors, MSCs).[4,5] Manufacturing MSCs with high energy density, long cycle life and fast charging/discharging rate at low cost remains a major challenge.[6] Albeit patterning methods such as template filtration,[7] lithography,[8] spray-masking and laser/plasma cutting[9,10] can partially meet the requirements, the involved lengthy procedures and material waste inevitably restrict these protocols from scalable production of

high-performance MSCs. This means that questing novel materials and developing scalable device patterning techniques at low cost are of significance and thus in high demand.

Compared to the abovementioned techniques, screen printing allows rapid, scalable fabrication of co-planar MSCs with reduction in material waste.[11,12] Among all other printing techniques, screen printing offers highest deposition rate (deposited material weight per unit time), especially if done in the roll-to-sheet mode. This is of particular interest for fabrication of energy storage devices with high areal capacitance. The major challenge consists in the development of functional inks with suitable rheological properties that allows high-resolution screen printing.[8,12–14] The solvent should be environmentally friendly so that the whole process is scalable and sustainable. To this end, great efforts have been made on screen printing of various functional inks based on one-dimensional carbon nanotubes,[15] two-dimensional (2D) graphene,[11,16] 2D layered double hydroxide,[17] transition metal dichalcogenide,[18] etc. Although devices printed from these inks feature good capacitance and cycle life,[17] quite limited success has been achieved on screen printing devices with high resolution and excellent charge storage/energy density/fast charging/discharging properties. In addition, most reported ink systems contain additives with the purpose either to boost electronic conductivity or to enhance the mechanical stability, adjust the rheological properties, or simply to increase the dispensability of the active materials.[12,13,19–21] Some other inks include a secondary solvent to tune the solidification speed as well as surface tension.[19,20] The presence of these additives requires additional removal processes (i.e. thermal annealing) which inevitably complicate the device manufacturing procedures. In other words, questing functional viscous inks in the absence of any additives at low cost for screen printing is of significance for scalable production of MSCs and other smart printed electronics.

MXenes are a new class of materials from the 2D family made of carbides and nitrides of transition metals (M), where X represents carbon and/or nitrogen.[22–24] MXenes are typically

obtained by selective removal of the A element (group 14 and 15, i.e. Al or Ga) from the MAX precursors.[25,26] Due to their exotic electrical, mechanical, thermal, optical properties and so forth,[27][28] MXenes, especially the most widely studied member $Ti_3C_2T_x$ (where T_x is surface termination groups), have quickly attracted huge research attention in many areas covering electrochemical energy storage,[29–36] electromagnetic interference shielding,[37,38] catalysis,[39] sensing,[40] transparent conductive films,[41] with excellent performances. By delaminating multi-layered $Ti_3C_2T_x$ (m-$Ti_3C_2T_x$), colloidal solutions composed predominantly of monolayered nanosheets are obtained, which can be further employed for inkjet or extrusion printing.[4,42,43] Recently, Han et al. reported screen printing of MSCs based on delaminated-MXene (d-MXene) inks, showcasing a specific capacitance of 52 F/g at a current density of 1 A/g in potassium hydroxide electrolyte.[17] By employing nitrogen-doped $Ti_3C_2T_x$ inks, Sun et al. demonstrated efficient printing of 3D electrodes based on delaminated MXene solutions for sodium-ion hybrid capacitors.[44] To date, there are a few reports on the screen printing of delaminated MXene inks for MSCs. Nevertheless, all screen-printed MXene MSCs with fine printing resolution and excellent charge storage properties have yet to be developed. Moreover, we note that, even after an efficient delamination of multilayered MXene (m-MXene), the weight percent of residues consisted of unetched MAX and un-exfoliated m-MXene can be up to 80-90%.[45,46] These sediments are typically trashed away, which surges the printing cost of MXene-based MSCs and wastes quite some amount of materials. This is especially true by taking the large amount of inks required by the screen printing technique into consideration.

Herein, we report on the ink formulation and scalable screen printing of MXene sediments. The MXene sediments after delamination are collected and formulated as screen-printable inks in the absence of any additives. We demonstrate the fine printed MXene-MSCs with excellent mechanical flexibility and areal capacitance/energy density. We also show efficient printing of various patterns, i.e., conductive tracks and integrated circuits, with high-resolution and spatial uniformity. We further demonstrate scalable screen printing based on MXene sediment inks,

suggesting the great potential of this printing platform for upscaling and sustainable production of next-generation wearable electronics.

MXene sediments ink formulation

We employed a less aggressive etching method, so-called minimally intensive layer delamination (MILD),[28,45] to remove the A element from the MAX phase, as shown in Supplementary Scheme 1. After etching, the morphology changes from compacted layered ceramics to a loose structure with apparent gaps among the sheets (Supplementary Figure 1), agreeing with previous reports and confirming the removal of aluminum from $Ti_3AlC_2T_x$.[45] After vigorous shaking and/or sonication of the m-$Ti_3C_2T_x$ suspension and subsequent centrifugation, mono- or few-layered $Ti_3C_2T_x$ nanosheets (supernatant) are separated from unetched MAX phase and un-exfoliated m-MXene (sediment) which leads to a substantial loss of material and surges up MXene synthesis costs, hampering the scalable production of MXene-based devices.[30,32,45–48] We note that this leads to a substantial loss of material and surges up MXene synthesis costs, hampering the scalable production of MXene-based devices. To this end, we formulate the "trashed" sediments by leaving a few percent of delaminated nanosheets when decanting the supernatant, and adding a small amount of DI-water, followed by a three-roll mill processing to form a homogeneous sediment ink, as detailed in Methods. Such modified "trashed" sediment inks are additive-free and are further employed for screen printing of various patterns, such as MSCs and conductive tracks, as demonstrated in Scheme 1.

We start by describing the ink characterizations. The as-obtained inks possess a viscous nature (inset of **Figure 1**A) and a very low loss factor at rest, as also confirmed by the almost stand still of the ink dropped on the glass substrate at an incline angle of 30° after 30 min (Figure 1A). Scanning electron microscope (SEM) images indicate the presence of delaminated nanosheets as well as layered particles in the inks (Figure1B,C). Figure 1D shows the transmission electron microscope (TEM) image, further verifying the existence of high-quality delaminated

nanosheets and m-$Ti_3C_2T_x$ in the inks. The atoms in the delaminated nanosheets show hexagonal packing behaviors (inset in Figure 1D). These delaminated nanosheets appear transparent to the electron beam, underlining their ultrathin nature. The dimensions of the flakes can be further confirmed by atomic force microscopy (AFM). The height profiles reveal lateral flake dimensions of ~4 μm and a thickness range of 1.5~6.5 nm (Figure 1E-F), corresponding to a layer number per sheets ranging from 1 to 4. Indeed, this small percentage of delaminated nanosheets (~2 wt.%) are left in the sediment on purpose to cross-bind the layered particles as well as adjusting the rheological properties. Based on the viscosity-shear rate plots in Figure 1G, the inks exhibit an apparent viscosity of 35 Pa·s coupled with non-Newtonian characteristics and shear-thinning (pseudoplastic) behaviour. The storage modulus and loss modulus were further measured to reveal the viscoelastic properties of the as-formulated inks. As shown in Figure 1H, the storage modulus is higher than the loss modulus when the strain is smaller than 40%, exhibiting the behavior of a typical elastic-like solid. Increasing the strain beyond 40% leads the loss modulus to be higher than the storage modulus, implying a transition from solid-like to liquid-like behavior.[49] It's worth noting that during printing, the aqueous inks gradually lose water and thus change their own rheological properties. For instance, after printing, the solid fraction increases to 34 wt.% with high apparent viscosity of 480 Pa·s and high storage modulus (Supplementary Figure 2), which are beyond the favorable ink rheological properties for the screen printing.

Screen-printed patterns

We then demonstrate the characterizations of screen-printed patterns. In printed electronics, the line gap and width with a straight shape are equally important for the realization of high-performance devices, such as interdigitated MSCs where straight lines with small gaps and narrow width are preferred to achieve high capacitance. By carefully designing the screens with predefined geometries, various conductive tracks with different line gaps can be quickly printed.

For instance, interdigitated MSCs consisting of straight lines with gap of 100 μm (Supplementary Figure 3A,B) and 200 μm (**Figure 2**A), respectively, were simply printed; In the printed lines, the surface exhibits some texture (Supplementary Figure 3A,B). This texture is partially caused by the screen mesh which is a common phenomenon in screen printed structures. When ink is transferred to the substrate, upon releasing of the mesh, ink will be dragged out by the mesh which can level out again if ink shows enough thixotropy. However, since paper absorbs ink's water rapidly, viscosity of the ink increases dramatically, and a rough surface is obtained. Existence of large particles (either unetched MAX phase or multilayer MXene) in the sediment ink is another reason for such a rough surface. Close examination of the printed lines reveals that m-MXene and MAX particles are well wrapped by the delaminated nanosheets (Figure 2B and Supplementary Figure 3C), forming a continuous metallic network. The small amount of delaminated nanosheets added to the sediments not only smoothens the line surface (Figure 2C and Supplementary Figure 3D), but also maintains good mechanical stability upon bending as well as provides good electron transport pathways with the printed lines, as will be discussed below. The X-ray diffraction pattern further confirms the presence of unetched MAX and un-exfoliated MXene particles, as well as delaminated nanosheets in the printed lines, best evidenced by the (002) peak centered at 6.8° (Supplementary Figure 4).

In printed electronics, printing resolution and spatial uniformity are of great importance.[4] Here we demonstrate that the as-obtained lines (width ~235 μm, number of printed passes, $<N>=3$) exhibit a high printing resolution with a spatial uniformity (averaged width variation based on the statistics) as low as 6%. Such a high printing resolution allows us to print various fine patterns, such as Switzerland's map, letters, QR codes, integrated circuit paths, etc. (Figure 2E), showcasing a great versatility of this screen-printing technique. By adjusting the printing passes, both thickness (measured with confocal microscopy, Supplementary Figure 5) and sheet resistance of the lines can be effectively tuned; multiple printed passes result in thicker films in general, and thus reduced sheet resistance. For instance, as increasing the printed pass from 1

to 6, the thickness boosts from 1.4 μm to 18 μm while the sheet resistance dramatically decreases from 16 ohm/sq to 2.2 ohm/sq (Figure 2F, G). Based on the thickness and sheet resistance, the electrical conductivity of printed lines was calculated, showing 260~450 S/cm, depending on the number of printed passes (Supplementary Figure 6). We note that the capability of multiple screen printing without compromising the printing resolution or flooding the interspace to the neighboring lines is of significance, enabling us to efficiently print thick films with better charge storage properties and higher rate performance.

To highlight the crucial role of the few percent of delaminate nanosheets, a control sample was obtained (with similar thickness) by screen printing solely the sediments without the inclusion of delaminated nanosheets. The sheet resistance of the control sample is >3 times higher (52.7 ohm/sq) than that of the printed line with d-MXene when $<N>=1$ (inset of Figure 2G). Moreover, upon bending the printed lines, the d-MXene nanosheets effectively behave as conductive binders which bridge the particles, thus avoid cracking by maintaining the mechanical integrity and leading to an almost constant resistance even when the lines were bent by 180° over a radius of 10 mm for couple of times (Figure 2H). On the contrary, the resistance of the as-printed line without d-MXene nanosheets increases drastically and decreases apparently upon bending and releasing, respectively. Repeated bending leads to an irreversible increase in resistance, best evidenced by the gradually increased resistance in the initial four cycles (Figure 2H). Such a difference is even more obvious when evaluating the long-term bending performance. As demonstrated in Figure 2I, the as-printed lines with the presence of d-MXene nanosheets exhibit stable resistance over 15,000 bending cycles, in sharp contrast to the control sample without d-MXene whose resistance increased by 182%. The electrical and mechanical flexibility results verify that the added d-MXene nanosheets to the sediment is crucial for the achievement of robust conductive lines with high printing resolution. In addition, one is able to screen print the as-formulated inks on paper and glass with almost identical Raman spectra (Figure 2J); all the spectra show the expected vibrational modes for the $Ti_3C_2T_x$

instead of anatase,[46] suggesting no oxidation was introduced during screen printing regardless of substrate. Characteristic peaks of MAX phase are not obvious, probably due to its small amount in the printed samples as well as highly overlapped peak positions as that of m-MXene.[23,50]

Charge storage performance of printed MSCs

We then evaluate the charge storage properties of the screen-printed MSCs as examples to demonstrate the possible use of this "turn trash into treasure" strategy. No additional current collectors or polymeric binders were used, all the MSCs were measured using a sulfuric acid (H_2SO_4)-poly(vinyl alcohol, PVA) gel electrolyte,[41] as shown in **Figure 3**A. The protons from the electrolyte interact with hydroxyl groups on the MXene, which further result in the continuous valence change of Ti (Figure 3B).[51] As such, $Ti_3C_2T_x$ MXene exhibits a pseudocapacitive behaviour when used as a supercapacitor electrode in acidic electrolyte. This is further verified by the normalized cyclic voltammograms (CVs) and galvanostatic charge-discharge (GCD) curves shown in Figure 3C,D, as rectangular CV shape and symmetric, linear GCD curves are observed, respectively, in the typical printed MSC (<*N*>=5, Gap=200 μm). Areal capacitances derived from CV and GCD profiles are plotted as a function of charge/discharge rates in Figure 3E. The values achieved from these two techniques are comparable and are well maintained when elevating the current density by 30 times (from 158 mF/cm^2 at 0.08 mA/cm^2 to 127 mF/cm^2 at 2.4 mA/cm^2), indicative of a high response rate. The pseudocapacitive charge storage behaviour is also confirmed by electrochemical impedance spectroscopy (EIS, Figure 3F). The Nyquist plot shows an electrolyte resistance of 27 Ω based on the intercept at high frequency region. After repeated GCD tests, the electrolyte resistance increases to 32 Ω (inset of Figure 3F). No semicircle is observed, suggesting the charge transfer resistance (R_{ct}) can be neglected. Importantly, the Nyquist plots exhibit almost vertical curves in the low frequency region, suggesting ideal capacitive behaviours, agreeing with the CV and

GCD results. The voltage window of screen-printed MSCs is limited to 0.6 V, highlighting the necessity of printing an asymmetric configuration to broaden the operation voltage window. In addition, the as-printed MSC showcases excellent mechanical resilience; the CV curve at 20 mV/s are well maintained even when bending to 180° (Figure 3G,H). After 1000 complete bending cycles, the CV integrated area decreases by 8% (Figure 3I), showcasing excellent mechanical flexibility of the device.

By optimizing the printed line gap as well as the number of printed passes (<*N*>), the charge storage properties can be tuned. Here we achieved this by engineering the pattern of the screens with different line gaps ranging from 200 to 500 μm. CVs and GCDs of printed MSCs with different gaps are shown in **Figure 4**A,B and Supplementary Figure 7A, indicating better charge storage performance when the gap is narrower. Almost all devices showcase excellent Coulombic efficiency (~97~99%) except the sample with gap=200 μm, <*N*>=5 one (~87%), which probably due to the mismatch of electrode height and/or sample impurities. Decreasing the line gap from 500 μm to 200 μm leads to a much enhanced areal capacitance by a factor of 1.83 (from 87 to 158 mF/cm^2) at 0.08 mA/cm^2 (Figure 4C). On the other hand, by multiple screen printing passes of as-formulated inks, MSCs with different line thickness (Figure 2F) can be obtained. The electrochemical responses of devices with different <*N*> are shown in Figure 4D,E and Supplementary Figure 7B. In general, increasing <*N*> from 1 to 5 results in an enhancement of areal capacitance from 27 mF/cm^2 to 158 mF/cm^2.

Importantly, our screen-printed MSCs have outperformed most other MSCs in terms of areal capacitance and energy density. As shown in Figure 4G, compared to MSCs based on laser-scribed d-$Ti_3C_2T_x$ (24~27 mF/cm^2),[10,52] LBL-printed graphene (19.8 mF/cm^2),[53] MnO_2/graphene (35 mF/cm^2),[54] and PANi/graphene (119 mF/cm^2),[55] our screen-printed MSCs based on MXene sediment inks possess much higher areal capacitance (158 mF/cm^2, <*N*>=5). The calculated energy density and power density of the typical MSC (<*N*>=5) reaches

as high as 1.64 μWh cm^{-2} and 778.3 μW cm^{-2}, respectively, which are orders of magnitude higher than those of MSCs based on rGO,[56] spray coated graphene,[57] and extrusion-printed MXene,[4] etc. (Figure 4H). The typical MSC also showcases excellent cycling performance, retaining 95.8% of initial capacitance after cycling 17000 times without parasitic reactions involved (Figure 4I and inset). The charge storage properties and energy/power density of our MSCs can be further optimized by either engineering the screens, tuning the m-MXene interlayer spacing/defects/surface chemistries, and/or printing asymmetric configurations. There are also dozens of MXene members other than $Ti_3C_2T_x$ to choose from,[58] opening up a great opportunity of achieving superior MSCs by simply screen printing of MXene "trashed" sediments.

Actually, inks with a lower degree of exfoliation may be even more preferred compared to the fully delaminated nanosheets inks especially when a moderate mechanical stability is expected from the printed films. Indeed, MXene sediment inks can be formulated with higher solid contents, leading to more material deposited on the substrate than delaminated inks upon screen printing at each print pass. Hence, for equal number of overprints, higher areal capacitance is achieved for the sediment ink. From the ion diffusion/intercalation kinetics point of view, by printing sediment inks, abundant voids are typically created among the coalesced particles. The conductive MAX filler and higher-capacitance m-MXene than d-MXene due to the larger sheet spacing in the former facilitate improved proton intercalation/diffusion kinetics, resulting in enhanced charge storage performance in the sediment ink based MSCs.

Finally, we demonstrate the scalable production by screen printing using the as-formulated inks. By designing patterns with different line gaps and shapes, hundreds of MSCs, conductive tracks and letters in high resolution can be rapidly printed within seconds (**Figure 5**A and Supplementary Figure 8). These all-printed MSCs can be readily connected in series and/or parallel, forming tandem devices to satisfy specific energy/power demands (Figure 5B). For

instance, all tandem devices (4S, 4P and 8S) showcase ideal capacitive behaviour with ignorable IR drop (Figure 5C,D and Supplementary Figure 9,10). The 8S tandem device is able to charge/discharge at a high rate (Figure 5D,E), indicating a small equivalent series resistance. The all-printed high-performance MSCs can readily power a bright light emitting diode (LED) (Figure 5F), demonstrating practical applications for screen printed MXene "trashed" sediments.

Conclusion

In summary, we demonstrate the formulation of additive-free MXene sediment inks and scalable printing of various patterns and structures with a high resolution and spatial uniformity. We find that the inclusion of a few percent of delaminated MXene nanosheets is of crucial importance in facilitating ink formulation while maintaining the continuous metallic network and mechanical integrity. The printed resilient MSCs demonstrate excellent charge storage performance, including high areal capacitance and high energy/power density, surpassing all printed MSCs known to date. Such a screen printing technique based on the MXene "trashed" sediments is waste-free, scalable and low-cost. For this reason it is of industrial relevance to areas like internet-of-things (IoTs), smart labels, smart packaging, etc., where cheaper and easy-to-integrate components are required. Considering the rich MXene family, we believe that the "turn trash into treasure" ink formulation strategy has a much broader scope of application. Owing to their excellent confirmed performance in energy storage, sensors, antennas, electromagnetic shielding, to name just a few, such inks are likely to gain growing importance.

Experimental Section

Experimental details including MAX etching, MXene delamination, screen design, screen printing of the electronics and their characterizations are listed in the Supporting Information.

Acknowledgements

This paper was written by C.F.Z. with contributions from all co-authors. We acknowledge funding from an Empa internal research grant. The authors gratefully acknowledge access to

the Coating Competence Center (CCC) facility and the scanning user lab (SUL) at Empa. Financial support from the project FOXIP in the framework of the Strategic Focus Area (SFA) Advanced Manufacturing of the ETH Board is acknowledged.

Conflict of interest

The authors declare no conflict of interest.

Keywords

Screen printing, additive manufacturing, MXene, conductive ink, microsupercapacitor

Received: ((will be filled in by the editorial staff))
Revised: ((will be filled in by the editorial staff))
Published online: ((will be filled in by the editorial staff))

[1] L. Kong, C. Zhang, J. Wang, D. Long, W. Qiao, L. Ling, *Mater. Chem. Phys.* **2015**, *149–150*, 495.

[2] Y. Wei, Y. Tao, C. Zhang, J. Wang, W. Qiao, L. Ling, D. Long, *Electrochim. Acta* **2016**, *188*, 385.

[3] J. Xiong, L. Pan, H. Wang, F. Du, Y. Chen, J. Yang, C. (John) Zhang, *Electrochim. Acta* **2018**, *268*, 503.

[4] C. (John) Zhang, L. McKeon, M. P. Kremer, S. H. Park, O. Ronan, A. Seral-Ascaso, S. Barwich, C. Coileáin, N. McEvoy, H. C. Nerl, B. Anasori, J. N. Coleman, Y. Gogotsi, V. Nicolosi, *Nat. Commun.* **2019**, *10*, 1795.

[5] D. Pech, M. Brunet, H. Durou, P. Huang, V. Mochalin, Y. Gogotsi, P.-L. Taberna, P. Simon, *Nat. Nanotechnol.* **2010**, *5*, 651.

[6] M. Beidaghi, Y. Gogotsi, *Energy Environ. Sci.* **2014**, *7*, 867.

[7] X. Wang, V. Raju, W. Luo, B. Wang, W. F. Stickle, X. Ji, *J. Mater. Chem. A* **2014**, *2*, 2901.

[8] L. Zhang, H. Liu, Y. Zhao, X. Sun, Y. Wen, Y. Guo, X. Gao, C. Di, G. Yu, Y. Liu, *Adv. Mater.* **2012**, *24*, 436.

[9] M. F. El-Kady, V. Strong, S. Dubin, R. B. Kaner, *Science* **2012**, *335*, 1326.

[10] Y.-Y. Peng, B. Akuzum, N. Kurra, M.-Q. Zhao, M. Alhabeb, B. Anasori, E. C. Kumbur, H. N. Alshareef, M.-D. Ger, Y. Gogotsi, *Energy Environ. Sci.* **2016**, *9*, 2847.

[11] W. J. Hyun, E. B. Secor, M. C. Hersam, C. D. Frisbie, L. F. Francis, *Adv. Mater.* **2015**, *27*, 109.

[12] G. Hu, J. Kang, L. W. T. Ng, X. Zhu, R. C. T. Howe, C. G. Jones, M. C. Hersam, T. Hasan, *Chem. Soc. Rev.* **2018**, *47*, 3265.

[13] G. Hu, T. Albrow-Owen, X. Jin, A. Ali, Y. Hu, R. C. T. Howe, K. Shehzad, Z. Yang, X. Zhu, R. I. Woodward, T.-C. Wu, H. Jussila, J.-B. Wu, P. Peng, P.-H. Tan, Z. Sun, E. J. R. Kelleher, M. Zhang, Y. Xu, T. Hasan, *Nat. Commun.* **2017**, *8*, 278.

[14] F. Torrisi, T. Hasan, W. Wu, Z. Sun, A. Lombardo, T. S. Kulmala, G.-W. Hsieh, S. Jung, F. Bonaccorso, P. J. Paul, D. Chu, A. C. Ferrari, *ACS Nano* **2012**, *6*, 2992.

[15] X. Cao, H. Chen, X. Gu, B. Liu, W. Wang, Y. Cao, F. Wu, C. Zhou, *ACS Nano* **2014**, *8*, 12769.

[16] E. B. Secor, S. Lim, H. Zhang, C. D. Frisbie, L. F. Francis, M. C. Hersam, *Adv. Mater.* **2014**, *26*, 4533.

[17] S. Xu, Y. Dall'Agnese, G. Wei, C. Zhang, Y. Gogotsi, W. Han, *Nano Energy* **2018**, *50*, 479.

[18] Y. D. Kim, J. Hone, *Nature* **2017**, *544*, 167.

[19] D. McManus, S. Vranic, F. Withers, V. Sanchez-Romaguera, M. Macucci, H. Yang, R. Sorrentino, K. Parvez, S.-K. Son, G. Iannaccone, K. Kostarelos, G. Fiori, C. Casiraghi, *Nat. Nanotechnol.* **2017**, *12*, 343.

[20] W. J. Hyun, E. B. Secor, C.-H. Kim, M. C. Hersam, L. F. Francis, C. D. Frisbie, *Adv. Energy Mater.* **2017**, *7*, 1700285.

[21] D. Song, A. Mahajan, E. B. Secor, M. C. Hersam, L. F. Francis, C. D. Frisbie, *ACS Nano* **2017**, *11*, 7431.

[22] B. Anasori, Y. Xie, M. Beidaghi, J. Lu, B. C. Hosler, L. Hultman, P. R. C. Kent, Y. Gogotsi, M. W. Barsoum, *ACS Nano* **2015**, *9*, 9507.

[23] M. Naguib, O. Mashtalir, J. Carle, V. Presser, J. Lu, L. Hultman, Y. Gogotsi, M. W. Barsoum, *ACS Nano* **2012**, *6*, 1322.

[24] H. Tang, W. Li, L. Pan, C. P. Cullen, Y. Liu, A. Pakdel, D. Long, J. Yang, N. McEvoy, G. S. Duesberg, V. Nicolosi, C. J. Zhang, *Adv. Sci.* **2018**, *4*, 1800502.

[25] M. Ghidiu, S. Kota, J. Halim, A. W. Sherwood, N. Nedfors, J. Rosen, V. N. Mochalin, M. W. Barsoum, *Chem. Mater.* **2017**, *29*, 1099.

[26] M. Naguib, V. N. Mochalin, M. W. Barsoum, Y. Gogotsi, *Adv. Mater.* **2014**, *26*, 992.

[27] C. (John) Zhang, V. Nicolosi, *Energy Storage Mater.* **2019**, *16*, 102.

[28] C. (John) Zhang, Y. Ma, X. Zhang, S. Abdolhosseinzadeh, H. Sheng, W. Lan, A. Pakdel, J. Heier, F. Nüesch, *ENERGY Environ. Mater.* **2019**, eem2.12058.

[29] M. Ghidiu, M. R. Lukatskaya, M.-Q. Zhao, Y. Gogotsi, M. W. Barsoum, *Nature* **2014**, *516*, 78.

[30] Y. Xia, T. S. Mathis, M.-Q. Zhao, B. Anasori, A. Dang, Z. Zhou, H. Cho, Y. Gogotsi, S. Yang, *Nature* **2018**, *557*, 409.

[31] M. R. Lukatskaya, S. Kota, Z. Lin, M.-Q. Zhao, N. Shpigel, M. D. Levi, J. Halim, P.-L. Taberna, M. W. Barsoum, P. Simon, Y. Gogotsi, *Nat. Energy* **2017**, *2*, 17105.

[32] M. R. Lukatskaya, O. Mashtalir, C. E. Ren, Y. Dall'Agnese, P. Rozier, P. L. Taberna, M. Naguib, P. Simon, M. W. Barsoum, Y. Gogotsi, *Science* **2013**, *341*, 1502.

[33] C. (John) Zhang, S. H. Park, A. Seral-Ascaso, S. Barwich, N. McEvoy, C. S. Boland, J. N. Coleman, Y. Gogotsi, V. Nicolosi, *Nat. Commun.* **2019**, *10*, 849.

[34] C. (John) Zhang, L. Cui, S. Abdolhosseinzadeh, J. Heier, *InfoMat* **2020**, inf2.12080.

[35] M. Shi, P. Xiao, J. Lang, C. Yan, X. Yan, *Adv. Sci.* **2020**, *7*, 1901975.

[36] Q. Jiang, N. Kurra, K. Maleski, Y. Lei, H. Liang, Y. Zhang, Y. Gogotsi, H. N. Alshareef, *Adv. Energy Mater.* **2019**, *9*, 1901061.

[37] F. Shahzad, M. Alhabeb, C. B. Hatter, B. Anasori, S. Man Hong, C. M. Koo, Y. Gogotsi, *Science* **2016**, *353*, 1137.

[38] J. Liu, H.-B. Zhang, R. Sun, Y. Liu, Z. Liu, A. Zhou, Z.-Z. Yu, *Adv. Mater.* **2017**, *29*, 1702367.

[39] Z. W. Seh, K. D. Fredrickson, B. Anasori, J. Kibsgaard, A. L. Strickler, M. R. Lukatskaya, Y. Gogotsi, T. F. Jaramillo, A. Vojvodic, *ACS Energy Lett.* **2016**, *1*, 589.

[40] Y.-Z. Zhang, K. H. Lee, D. H. Anjum, R. Sougrat, Q. Jiang, H. Kim, H. N. Alshareef, *Sci. Adv.* **2018**, *4*, eaat0098.

[41] C. J. Zhang, B. Anasori, A. Seral-Ascaso, S.-H. Park, N. McEvoy, A. Shmeliov, G. S. Duesberg, J. N. Coleman, Y. Gogotsi, V. Nicolosi, *Adv. Mater.* **2017**, *29*, 1702678.

[42] C. J. Zhang, M. P. Kremer, A. Seral-Ascaso, S.-H. Park, N. McEvoy, B. Anasori, Y. Gogotsi, V. Nicolosi, *Adv. Funct. Mater.* **2018**, *28*, 1705506.

[43] J. Orangi, F. Hamade, V. A. Davis, M. Beidaghi, *ACS Nano* **2020**, *14*, 640.

[44] L. Yu, Z. Fan, Y. Shao, Z. Tian, J. Sun, Z. Liu, *Adv. Energy Mater.* **2019**, *9*, 1901839.

[45] M. Alhabeb, K. Maleski, B. Anasori, P. Lelyukh, L. Clark, S. Sin, Y. Gogotsi, *Chem. Mater.* **2017**, *29*, 7633.

[46] C. J. Zhang, S. Pinilla, N. McEvoy, C. P. Cullen, B. Anasori, E. Long, S.-H. Park, A. Seral-Ascaso, A. Shmeliov, D. Krishnan, C. Morant, X. Liu, G. S. Duesberg, Y. Gogotsi, V. Nicolosi, *Chem. Mater.* **2017**, *29*, 4848.

[47] M. Mariano, O. Mashtalir, F. Q. Antonio, W.-H. Ryu, B. Deng, F. Xia, Y. Gogotsi, A. D. Taylor, *Nanoscale* **2016**, *8*, 16371.

[48] X. Zhang, C. (John) Zhang, A. Abas, Y. Zhang, X. Mu, J. Zhou, Q. Su, W. Lan, E. Xie, *Electrochim. Acta* **2019**, *296*, 535.

[49] Z. Fan, C. Wei, L. Yu, Z. Xia, J. Cai, Z. Tian, G. Zou, S. X. Dou, J. Sun, *ACS Nano* **2020**, acsnano.9b08030.

[50] M. Naguib, M. Kurtoglu, V. Presser, J. Lu, J. Niu, M. Heon, L. Hultman, Y. Gogotsi,

M. W. Barsoum, *Adv. Mater.* **2011**, *23*, 4248.

[51] M. Hu, Z. Li, T. Hu, S. Zhu, C. Zhang, X. Wang, *ACS Nano* **2016**, *10*, 11344.

[52] N. Kurra, B. Ahmed, Y. Gogotsi, H. N. Alshareef, *Adv. Energy Mater.* **2016**, *6*, 1601372.

[53] G. Sun, J. An, C. K. Chua, H. Pang, J. Zhang, P. Chen, *Electrochem. commun.* **2015**, *51*, 33.

[54] M. F. El-Kady, M. Ihns, M. Li, J. Y. Hwang, M. F. Mousavi, L. Chaney, A. T. Lech, R. B. Kaner, *Proc. Natl. Acad. Sci.* **2015**, *112*, 4233.

[55] Z.-S. Wu, K. Parvez, S. Li, S. Yang, Z. Liu, S. Liu, X. Feng, K. Müllen, *Adv. Mater.* **2015**, *27*, 4054.

[56] J. J. Yoo, K. Balakrishnan, J. Huang, V. Meunier, B. G. Sumpter, A. Srivastava, M. Conway, A. L. Mohana Reddy, J. Yu, R. Vajtai, P. M. Ajayan, *Nano Lett.* **2011**, *11*, 1423.

[57] H. Li, Y. Hou, F. Wang, M. R. Lohe, X. Zhuang, L. Niu, X. Feng, *Adv. Energy Mater.* **2017**, *7*, 1601847.

[58] B. Anasori, M. R. Lukatskaya, Y. Gogotsi, *Nat. Rev. Mater.* **2017**, *2*, 16098.

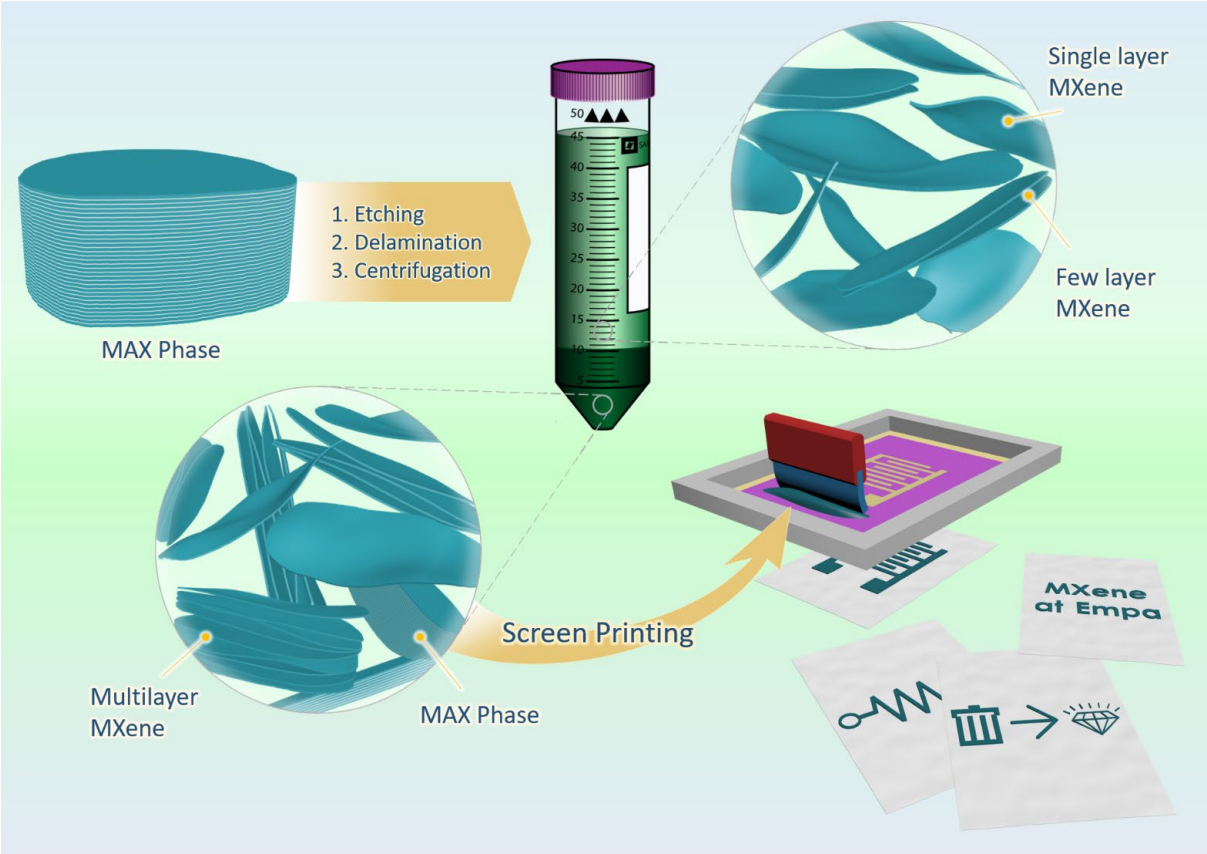

Scheme 1. Schematic illustration of direct screen printing of MXene sediments. After centrifugation, solely the delaminated few-layered $Ti_3C_2T_x$ MXene nanosheets solution (in the supernatant) is generally collected, while the sediments consisting of multi-layered $Ti_3C_2T_x$ MXene and unetched Ti_3AlC_2 MAX phases are typically discarded as "trash". By collecting the "trash" and tuning their viscosity properties, the sediment inks are used for screen printing of various patterns, such as letters, conductive wires, MSCs and other patterns. As for the MSCs, a gel electrolyte made of H_2SO_4-PVA, was coated onto the as-printed patterns and dried at ambient condition for 6 h, forming solid-state MSCs.

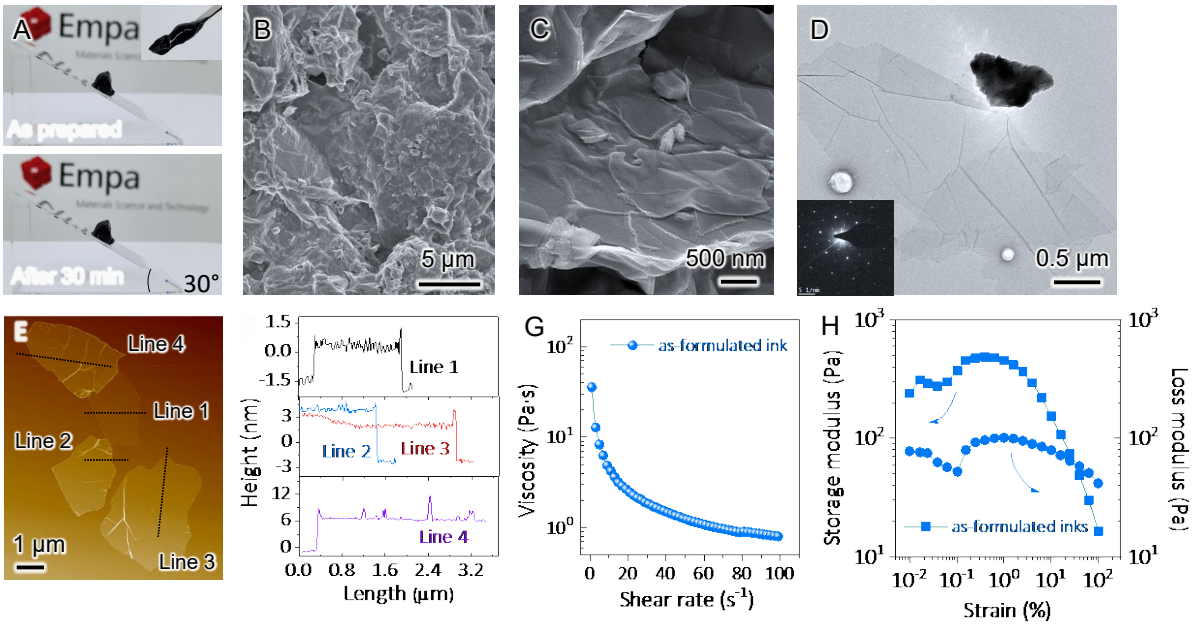

Figure 1. Characterizations of MXene sediment inks. (A), Photos of as-prepared MXene sediment inks (top and the inset) and dried at ambient condition for 30 min (bottom), showing a highly viscous nature. SEM images of the as-prepared MXene sediments at a low (B) and high (C) magnification, respectively, showing the smooth surface due to the presence of few-layered MXene nanosheets that act as conductive binder. (D), TEM image of MXene sediment inks. Inset shows the selected area electron diffraction (SAED) pattern. (E), AFM image and (F), the corresponding height profiles along the lines in (E). (G), Viscosity plotted as a function of shear rates of as-formulated MXene inks. (H), Storage modulus and loss modulus plotted as a function of strain of as-formulated MXene inks.

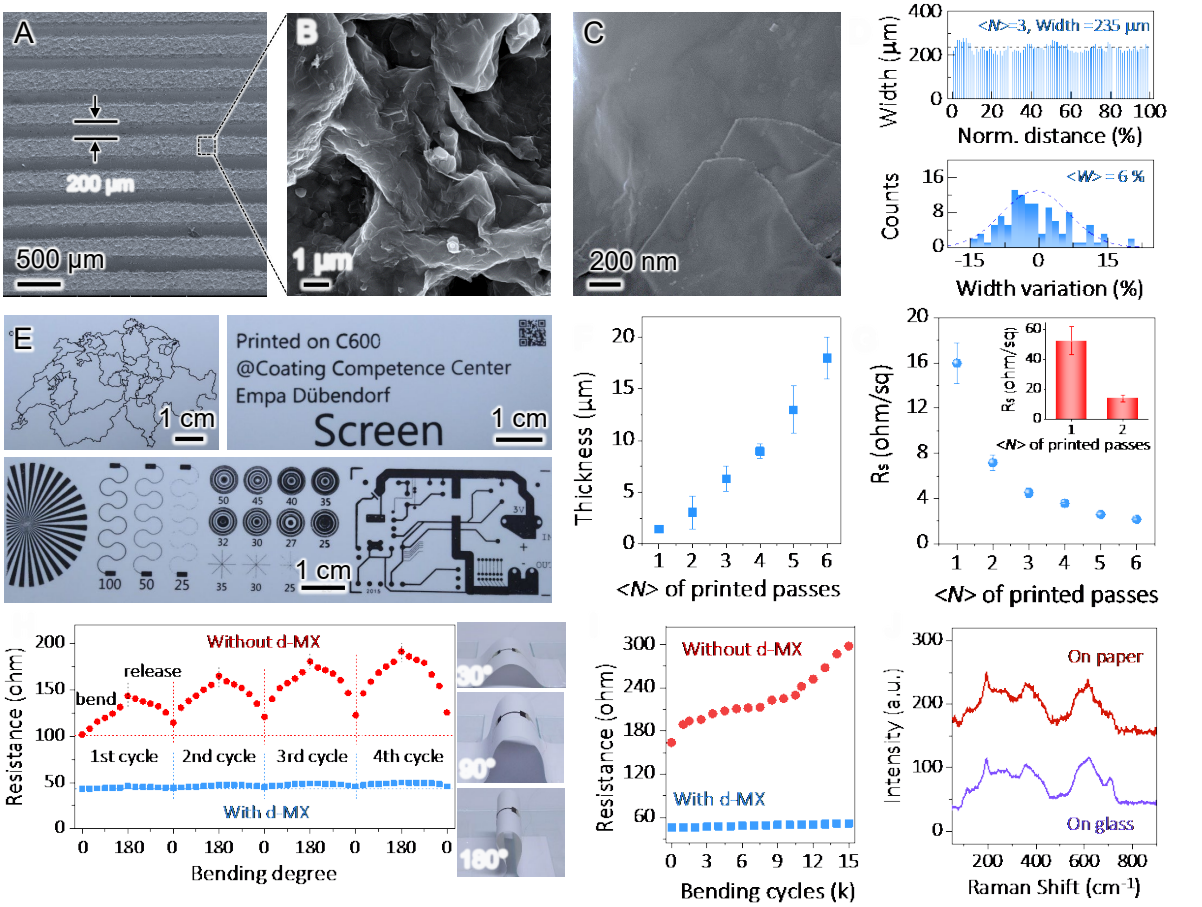

Figure 2. Screen printing of MXene sediment inks. (A-C), SEM images of screen-printed lines with different magnifications. (D), Width distribution (top) and variation distribution (bottom) of MXene printed lines with <*N*>=3. The narrow width distribution indicates a high printing resolution corresponding to a spatial uniformity of <W> of 6%. (E), Various screen-printed patterns, including a Switzerland's map (top left), letters (top right), conductive tracks, integrated circuits (bottom), etc. The line thickness (F) and sheet resistance (G) plotted as a function of <*N*>, respectively. The inset in (G) is the as-printed lines using the sediment ink without d-MXene nanosheets. Resistance change at different bending degrees (H) and bending cycles (I) of the as-printed lines from sediment inks with/without d-MXene nanosheets. One cycle is defined as bending the printed line to 180° and then releasing to 0° (flat). The right panel in H shows the optical images of as-printed line (2 cm in length) at different bending degrees based on the sediment inks with d-MXene nanosheets. (J) Raman spectra of as-printed lines on paper and glass and comparison to that of pure MXene film.

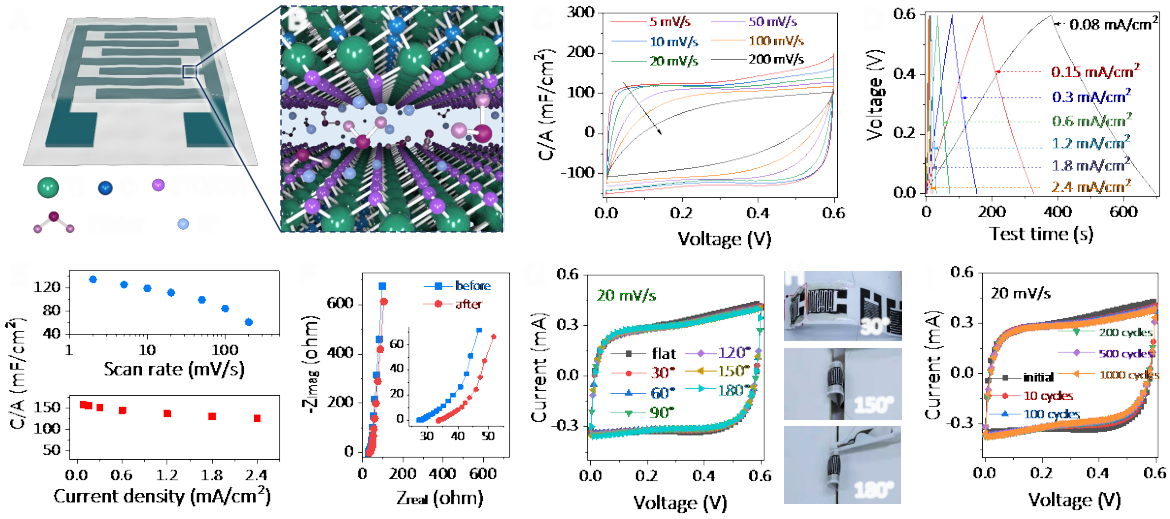

Figure 3. Electrochemical characterization of screen-printed MXene micro-supercapacitors. (A), Scheme of as-printed MXene-based microsupercapacitor, indicating the pseudocapative energy storage mechanism induced by the protons interacting with OH groups-terminated Ti (B). (C), Normalized cyclic voltammogram (CV) profiles and (D), Galvanostatic charge-discharge (GCD) curves of a typical screen-printed MSC (<*N*>=3, gap=200 µm). (E), Areal capacitance (C/A) of screen-printed MSC obtained via CV and GCD, respectively, showing similar values. (F), Electrochemical impedance spectroscopy of screen-printed MSC before and after the CV tests at various scan rates. CVs of screen-printed MSC under different bending degrees (G, H) and bending cycles (I) at 20 mV/s.

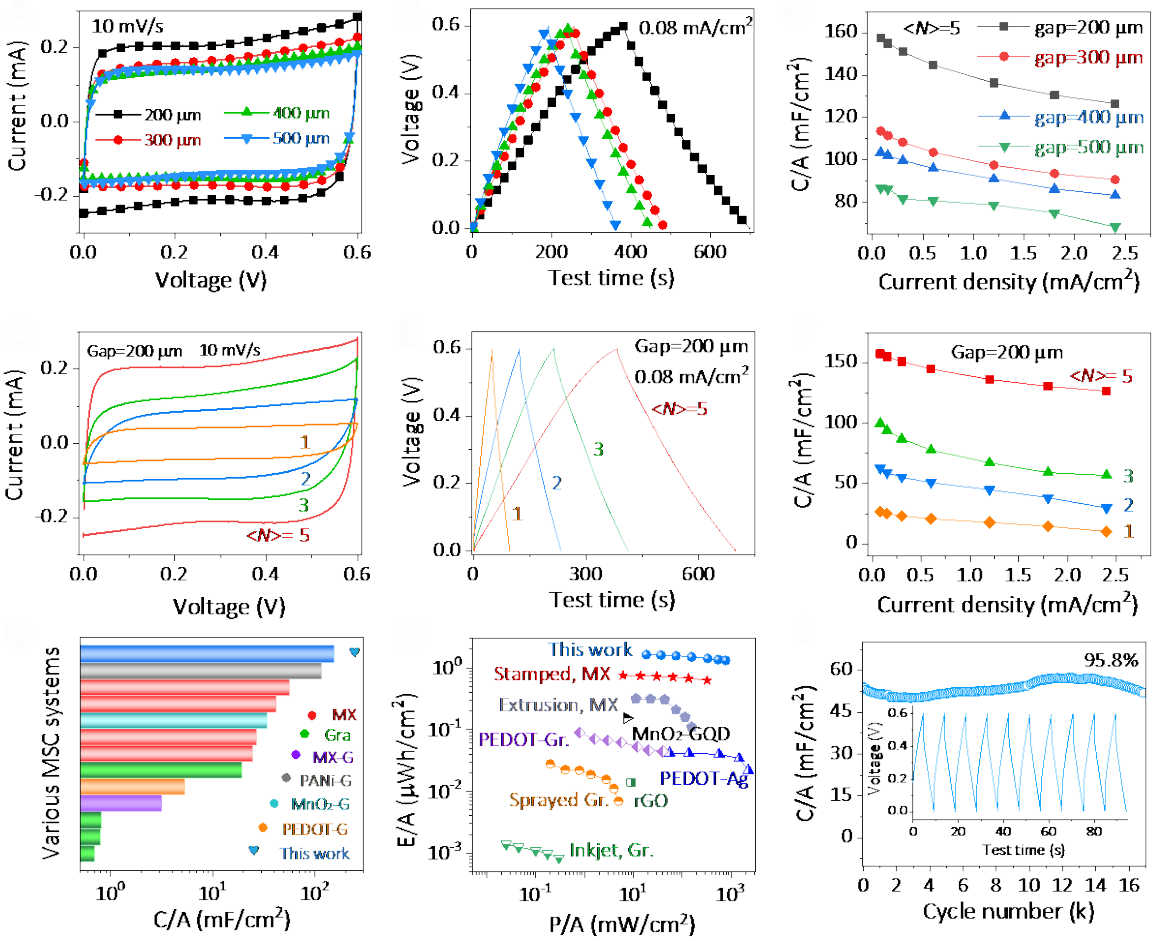

Figure 4. Effects of device configuration on the electrochemical performance. CV curves (A), GCD profiles (B) and areal capacitance (C) of screen-printed MSCs with different finger gaps (<*N*>=5). CV curves (D), GCD profiles (E) and areal capacitance (F) of MSCs with different number of printed passes (<*N*>). (G), Areal capacitance (C/A) comparison of this work to other reported MSC systems, showing much higher C/A of our printed MXene MSCs than other reports. (H), Ragone plot comparison of this work (screen-printed MSC with <*N*>=3) to other MSC systems. Detailed references and specific values in (G-H) can be found in the Supplementary Information. (I), Long-term cycling of screen-printed MSC. Inset is the typical GCD curves, showing capacitive behaviour during cycling, indicating that the excellent electrochemical performance is not due to parasitic reactions.

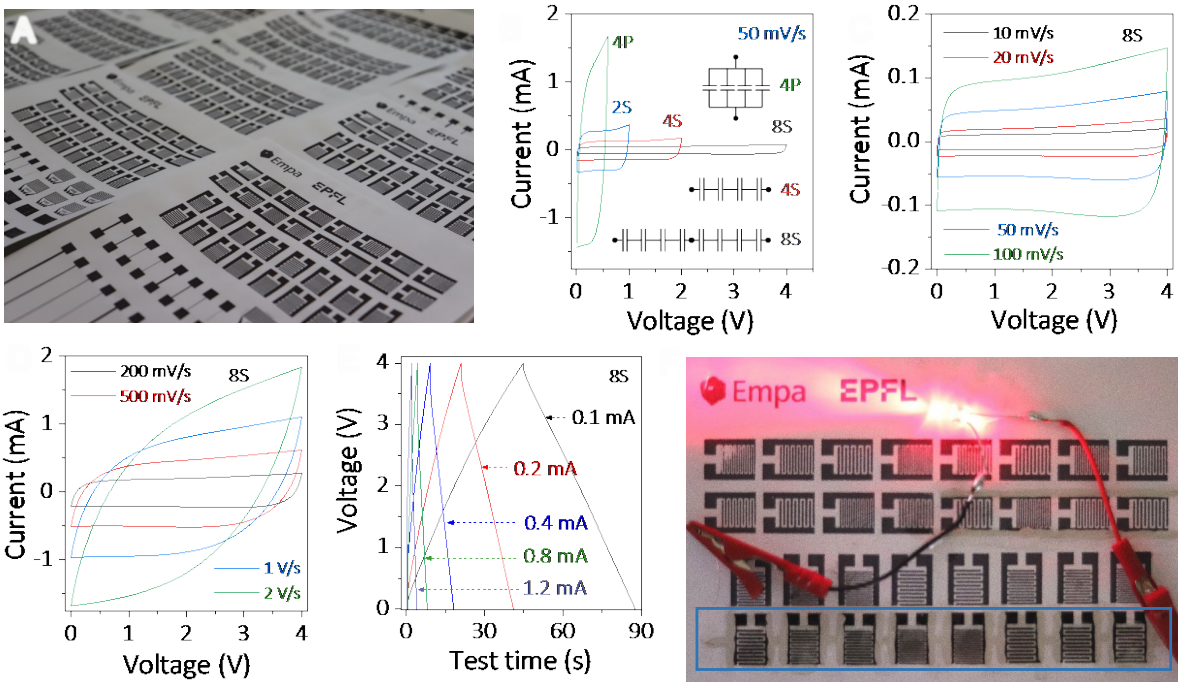

Figure 5. Scalable production of micro-supercapacitors based on MXene sediment inks. (A), Optical image of screen-printed MXene-based microsupercapacitor, showing the great promise of scale-up production of high-performance MSCs. (B), CV profiles of different tandem devices at 50 mV/s. (C-D), CVs of a tandem device with 8 MSCs connected in series at different scan rates, showing a high-rate response. (E), GCD profiles of a tandem device with 8 MSCs connected in series, indicating symmetric, linear curves at various currents. (F), Optical image of the tandem device to power a LED light, demonstrating the feasibility of the as-printed tandem device for practical applications.